Materials Chemistry and Physics 132 (2012) 187–191

Contents lists available at SciVerse ScienceDirect

Materials Chemistry and Physics

journal homepage: www.elsevier.com/locate/matchemphys

Formation and electrochemical behavior of Al and O plasma-implanted biodegradable Mg-Y-RE alloy

Ying Zhao [a,b], Guosong Wu [b], Haobo Pan [a], Kelvin W.K. Yeung [a,*], Paul K. Chu [b,*]

[a] Department of Orthopaedics & Traumatology, The University of Hong Kong, Pokfulam Road, Hong Kong
[b] Department of Physics and Materials Science, City University of Hong Kong, Tat Chee Avenue, Kowloon, Hong Kong

ARTICLE INFO

Article history:
Received 23 July 2011
Received in revised form 25 October 2011
Accepted 13 November 2011

Keywords:
A. Biomaterials
B. Surface
C. Ion implantation
D. Corrosion
E. Magnesium alloys

ABSTRACT

Mg-Y-RE alloy is potentially useful in biodegradable implants but the fast degradation rate in the physiological environment restrains actual applications. In order to enhance the corrosion resistance, aluminum and oxygen ion implantation is employed to modify the surface of the Mg-Y-RE alloy. X-ray photoelectron spectroscopy (XPS) is conducted to obtain elemental depth profiles and determine chemical state changes. Electrochemical impedance spectroscopy and potentiodynamic polarization are employed to investigate the electrochemical behavior in simulated body fluids (SBF). After polarization, the corroded surface is further studied by scanning electron microscopy (SEM). The results indicate Al and O ion implantation produces an Al_2O_3-containing protection layer which improves the corrosion resistance of Mg-Y-RE alloy. After the surface treatment, localized corrosion becomes the dominant corrosion mechanism instead of general corrosion.

1. Introduction

Magnesium as a degradable implant material provides both good biocompatibility and suitable mechanical properties as observed from earlier clinical examples as well as *in vitro* and *in vivo* assessments [1–8]. Among the various magnesium alloys, the Mg-Y-RE (WE43) alloy is one of the most promising candidates for biomedical degradable stents [9–11]. Yttrium (Y) and rare earth (RE) elements introduced into magnesium alloys are predominantly used to strengthen the materials and improve the corrosion resistance. In comparison with conventional stainless steels, stents made of WE43 possess superior antiproliferative properties and significantly decreased restenosis rate [11]. However, magnesium stents may degrade so quickly that arteries are not supported long enough to prevent negative remodeling [12]. Therefore, further protection has to be conducted to control the corrosion rate *in vivo* before WE43 can be safely applied to clinical applications [13].

Surface modification is a viable approach to make biodegradable Mg alloys more suitable for biomedical applications and has attracted growing interests [14–17]. Besides usual coating techniques, ion implantation can be utilized to control the degradation rate of magnesium and its alloys [18–22]. As a non-line-of-sight technique, plasma immersion ion implantation (PIII) is particularly suitable for magnesium alloy stents with a complex geometry [23,24]. Since the implanted layer which can be tailored is usually not very thick, it is possible to use ion implantation to adjust the degradation rate of biomedical magnesium alloys in a controllable manner, particularly in the early stage after surgery [25].

Generally, magnesium and magnesium alloys are prone to rapid surface oxidization when they are exposed to air because of their high chemical reactivity. Unfortunately, the oxide layer formed is usually loose and not stable in the aqueous medium thus affecting the protection ability [26]. Among the various structures, Al_2O_3 as a bioinert ceramic which has many clinical applications such as total hip prostheses and dental implants offers excellent hardness, high chemical stability, suitable tribological properties, as well as desirable biocompatibility [27–32]. Therefore, in order to improve the surface corrosion resistance, an Al_2O_3 layer is produced on the surface of the WE43 magnesium alloy by plasma immersion ion implantation in this study. Owing to the mismatch in the mechanical properties between Al_2O_3 and Mg and very negative electrochemical potential of Mg [26,33], an implanted Al layer serves as a transition layer between the Al_2O_3 layer and magnesium substrate. The electrochemical behavior and corresponding corrosion mechanism of the surface-treated alloy are investigated systematically in simulated body fluids (SBF).

2. Experimental details

As-cast WE43 plates (Mg with 4 wt% Y and 3 wt% Nd; 10 mm × 10 mm × 5 mm) were mechanically polished using up to

* Corresponding authors.
E-mail addresses: wkkyeung@hku.hk (K.W.K. Yeung), paul.chu@cityu.edu.hk (P.K. Chu).

0254-0584/$ – see front matter © 2011 Elsevier B.V. All rights reserved.
doi:10.1016/j.matchemphys.2011.11.028

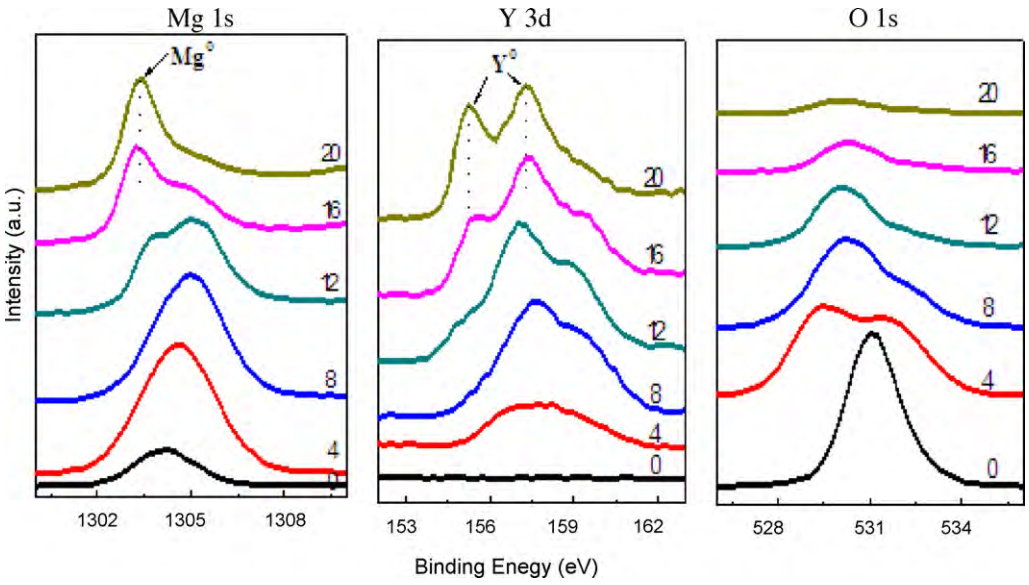

Fig. 1. High-resolution XPS spectra acquired from the WE43 magnesium alloys at different sputtering time with the numbers in the figures denoting the sputtering time.

5 μm diamond paste, ultrasonically washed in pure acetone and ethanol, and dried. Aluminum plasma ion implantation was carried out on the HEMII-80 ion implanter equipped with an aluminum cathodic arc source in the Plasma Laboratory in City University of Hong Kong. The samples were implanted for 1 h at a terminal acceleration voltage of 35 kV and base pressure of 1.5×10^{-3} Pa. The Al implanted samples then underwent oxygen ion implantation in a GPI-100 ion implanter. An oxygen plasma was formed in the chamber using an oxygen flow rate of 20 sccm. Using pulsed voltage, pulse width, and pulsing frequency of 20 kV, 50 μs, and 100 Hz, respectively, oxygen plasma immersion ion implantation was conducted for 3 h.

X-ray photoelectron spectroscopy (XPS) with Al Kα irradiation was used to determine the chemical states and elemental depth profiles before and after ion implantation. The sputtering rate was estimated to be about 7.6 nm min^{-1} based on that calculated from a SiO_2 standard sputtered under similar conditions. The binding energies were referenced to the C 1s line at 285.0 eV. The electrochemical experiments were performed in a simulated body fluid (SBF) with a pH of 7.40 (ion concentrations of Na^+ 142.0, K^+ 5.0, Mg^{2+} 1.5, Ca^{2+} 2.5, Cl^- 147.8, HCO_3^- 4.2, HPO_4^{2-} 1.0, and SO_4^{2-} 0.5 mM similar to those of human blood plasma [34]) at 37 °C on a Zahner Zennium electrochemical workstation using the conventional three-electrode technique. The potential was referred to a saturated calomel electrode (SCE) and the counter electrode was a platinum sheet. The specimens with a surface area of 10 mm × 10 mm were exposed to the SBF solution at 37 °C. The EIS data were recorded from 100 kHz to 100 mHz with a 10 mV sinusoidal perturbing signal at the open-circuit potential after stabilization in the solution for 5 min. The polarization curves were acquired by scanning the potential at a rate of 1 mV s^{-1} from −150 mV to 600 mV following the EIS measurement. After the polarization test, the surface morphology was examined by scanning electron microscopy (SEM).

3. Results and discussion

Fig. 1 illustrates the chemical state changes in the near surface of the un-implanted WE43 magnesium alloy. As shown in the high-resolution XPS spectra, the valence states of Mg and Y gradually change from the oxidized to metallic ones upon sputtering. In the meantime, the intensity of the O 1s peak declines gradually. It can thus be inferred that both Mg and Y are oxidized in the near surface. As reported in the literature, $Mg(OH)_2$ and MgO are usually formed on the surface of magnesium alloys after exposure to air [35]. In the WE43 alloy, $Mg_{12}YNd$ and $Mg_{14}YNd_2$ are the main precipitated phases [36]. Hence, Mg and the RE elements exist in many chemical states. Since some of them have approximate binding energy, it is difficult to ascertain their existence by XPS. Therefore, we only describe them as metallic Mg (Y or Al) or oxidized Mg (Y or Al) in this paper.

The elemental depth profiles obtained from the un-implanted WE43 alloy are depicted in Fig. 2. According to the chemical states of the elements, three different regions can be delineated in the near surface as follows: Region 1 (Mg^{n+}), Region 2 (Mg^{n+}, Mg^0, Y^{n+}, Y^0), and Region 3 (Mg^0, Y^0). The top surface layer is composed of magnesium compounds and its thickness is estimated to be about 15 nm. The amount of Y^{n+} in the top surface is relatively small and the thickness of the Y^{n+}-containing layer is about 150 nm.

Fig. 3 displays the chemical state changes in the Al–O implanted WE43 magnesium alloy versus sputtering time and Fig. 4 presents

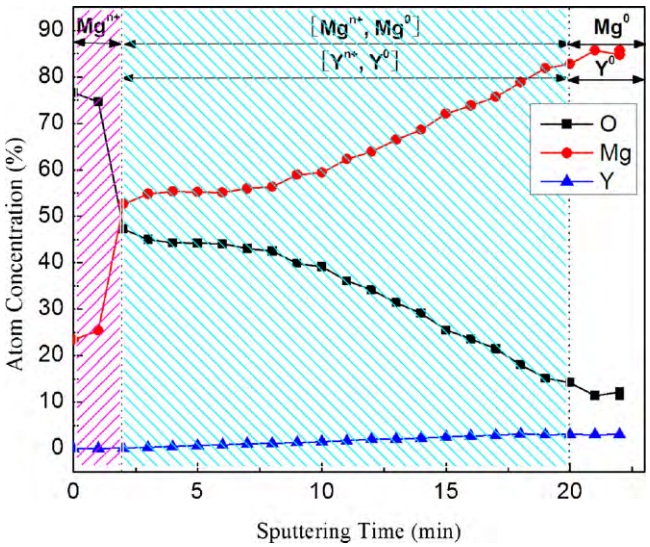

Fig. 2. XPS depth profile of WE43 magnesium alloy.

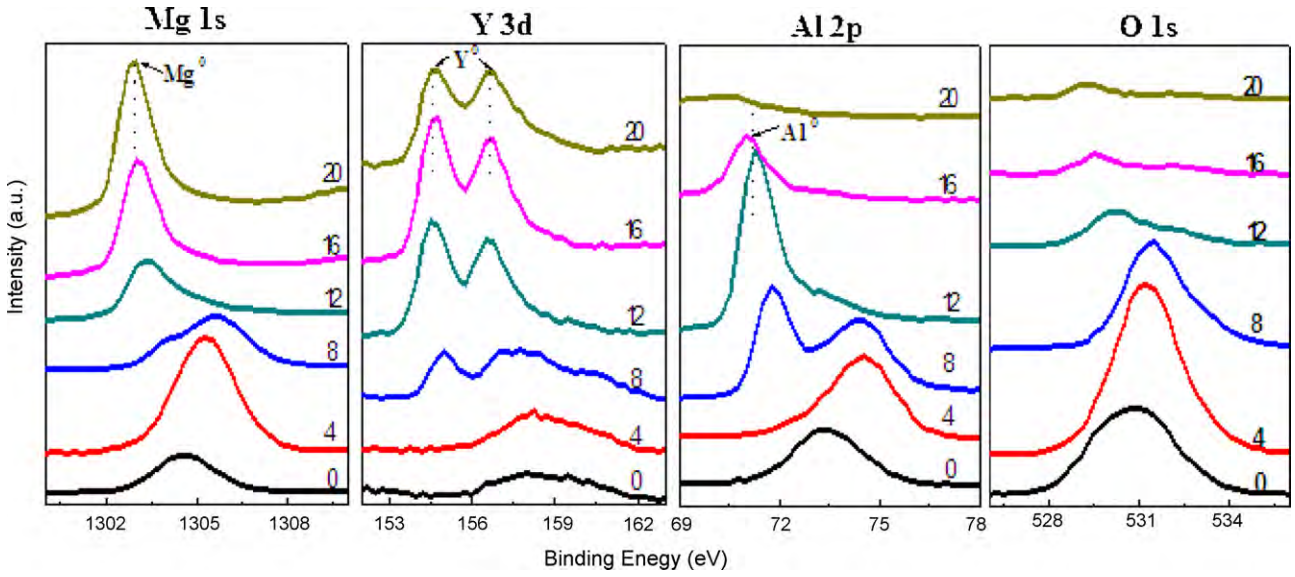

Fig. 3. High-resolution XPS spectra of WE43 magnesium alloys at different sputtering time after Al and O plasma ion implantation and the numbers in the figures denoting the sputtering time.

the XPS depth profiles. Following the analysis of Fig. 1, metallic Mg, Y and Al are indicated and designated as Mg^0, Y^0 and Al^0 in Fig. 3. In Fig. 4, six different regions in the near surface can be identified based on the chemical shifts revealed in Fig. 3. From the top surface to the bulk, they are: Region 1 (Mg^{n+}, Al^{n+}), Region 2 (Mg^{n+}, Al^{n+}, Al^0), Region 3 (Mg^{n+}, Mg^0, Y^{n+}, Y^0, Al^{n+}, Al^0), Region 4 (Mg^0, Y^0, Al^{n+}, Al^0), Region 5 (Mg^0, Y^0, Al^0), and Region 6 (Mg^0, Y^0). During ion implantation, Al and O ions penetrate the native surface oxide layer shown in Fig. 2 into the substrate. A gradient structure consisting of Al_2O_3-containing and Al-containing layers is formed near the surface after ion implantation. The implanted Al exhibits a Gaussian-like distribution with a peak concentration of about 40 at% and the Mg concentration is sharper in the implanted layer. Even though the thickness of the implanted layer is similar to that of the native oxide, the two structures are very different. In the implanted layer, Al^{n+} exists from Regions 1 to 4 to act as a barrier preventing metallic Mg from oxidation.

Fig. 5 displays the representative potentiodynamic polarization curves of the samples acquired in SBF. Generally, the corrosion potential and corrosion current density can be derived directly from the region in the cathodic polarization curves by Tafel region extrapolarization. Based on our calculation, the un-implanted sample has a fairly negative corrosion potential in SBF of about −1.972 V. Compared to the un-implanted sample, the corrosion potential of the implanted sample is nobler and shifts to about −1.586 mV. The corrosion resistance is closely related to the corrosion current density. The corrosion current density of the implanted sample (4.468×10^{-5} A cm^{-2}) is much lower than that of the un-implanted sample (6.025×10^{-4} A cm^{-2}), implying that degradation of magnesium is indeed retarded by ion implantation.

Fig. 6 shows the SEM micrographs of the WE43 magnesium alloy after polarization tests in SBF. General corrosion can be observed from the surface of the un-implanted sample as manifested by networks of cracks whereas localized corrosion is dominant on the Al–O implanted samples. The formation of cracks on the un-implanted samples may be due to dehydration of the corrosion

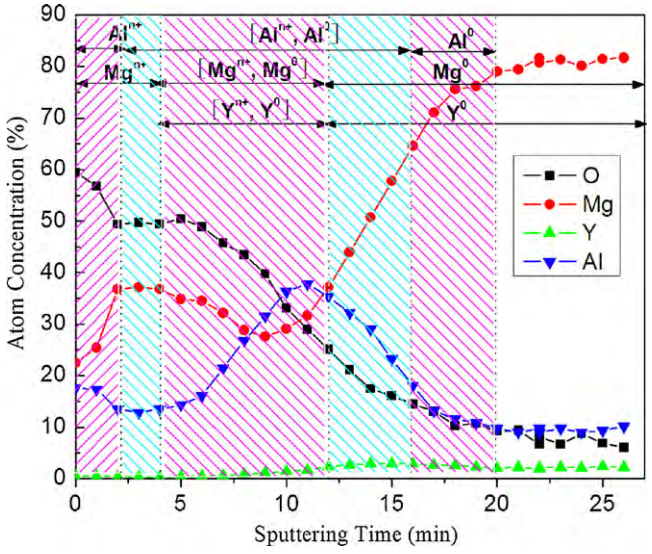

Fig. 4. XPS depth profile of WE43 magnesium alloy after Al and O plasma ion implantation.

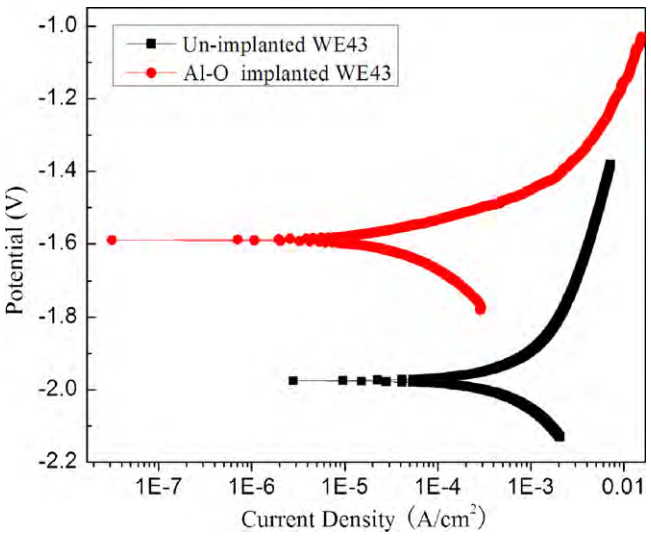

Fig. 5. Polarization curves of WE43 and Al–O implanted WE43 in SBF.

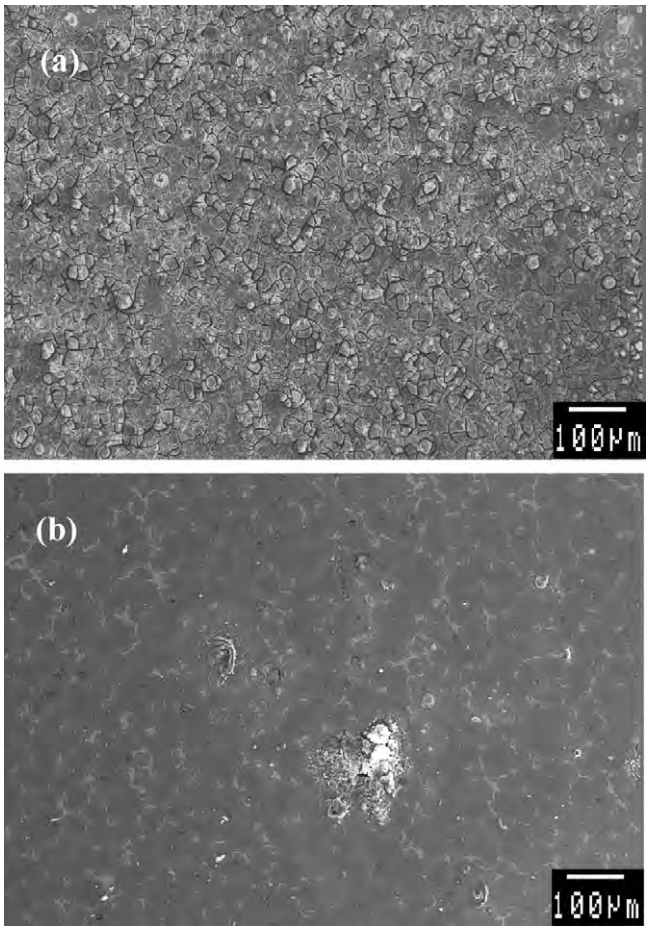

Fig. 6. SEM micrographs of magnesium alloys after polarization test in simulated body fluid: (a) un-implanted WE43 alloy and (b) Al–O implanted WE43 alloy.

products [37]. After ion implantation, the cracks almost disappear with the exception of some corrosion pits. Severe corrosion usually increases the possibility of cracks. Thus, our data imply that the corrosion resistance in SBF is improved after ion implantation. During attack by aggressive electrolytes, the protection offered by the implanted layer deteriorates and so some local corrosion occurs in the weak areas, but good corrosion is still observed from the undamaged regions.

Fig. 7 depicts the EIS spectra of the WE43 magnesium alloy after immersion in SBF for 5 min. Two capacitive arcs are shown from the curves of the un-implanted WE43 magnesium alloy, one in the high frequency region and the other in the low frequency region. When the sample is immersed in SBF, corrosion takes place on the entire surface and a corroded layer forms quickly. The capacitive arcs are usually attributed to charge transfer, film effects, as well as mass transfer in the corrosion product layer. After ion implantation, the capacitive arc is evidently enlarged, indicating that the corrosion rate of the implanted sample is significantly reduced. It is noted that the spectral shapes before and after ion implantation are different thereby providing clues about the different corrosion mechanisms. With regard to the implanted sample, the capacitive arc in the low frequency region is much smaller than that in the high frequency region. It may be related to corrosion taking place on the localized surface as shown in Fig. 6. The high frequency behavior in the EIS result is usually associated with electrolyte penetration including water uptake and salt intrusion. The low-frequency region in the EIS result contains important information about the electrode controlled process together with the contribution from localized defects to the overall impedance [38]. Considering the physical

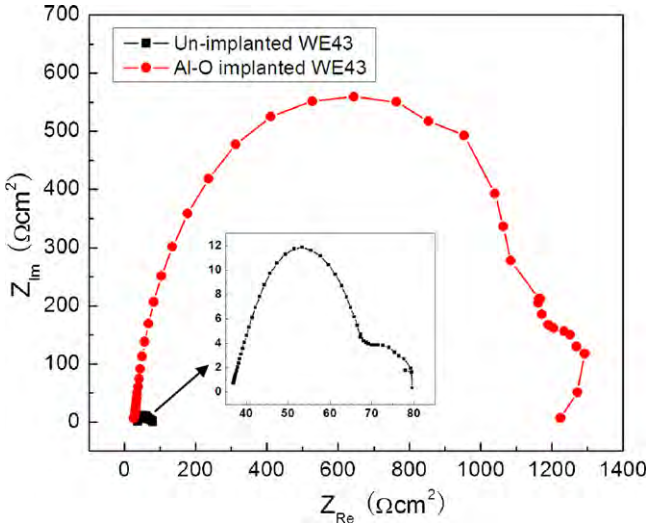

Fig. 7. Representative EIS spectra (Nyquist plots) of WE43 magnesium alloy after soaking in SBF for 5 min.

structure of the electrode system and its impedance response, an equivalent circuit to model the implanted alloy/solution system and the corresponding EIS fitting data are presented in Fig. 8 and Table 1. Here, C_f, one of the constant phase element (CPE) components, represents the capacitance of the corrosion product layer and R_f is the corresponding layer resistance. C_{dl}, another component of CPE, expresses the capacitance of the double layer in the vulnerable regions. R_t is the charge transfer resistance related to the electrochemical reaction in the same region and R_s, which is placed in series with other elements of the circuit, is the solution resistance between the reference and working electrodes. Its value depends on the conductivity of the test medium and geometry of the cell. R_{pore} is the sum of the resistances of all the pores in the corrosion product. For the Al–O implanted sample, both R_t and impedance of C_{dl} increase largely after implantation. Moreover, R_{pore} is significantly enhanced compared to R_f before implantation. They are in good agreement with the localized corrosion and general corrosion shown in Fig. 6. The results also reveal that the corrosion rate of the implanted sample diminishes significantly and it can be attributed to the formation of the Al_2O_3-containing oxide layer.

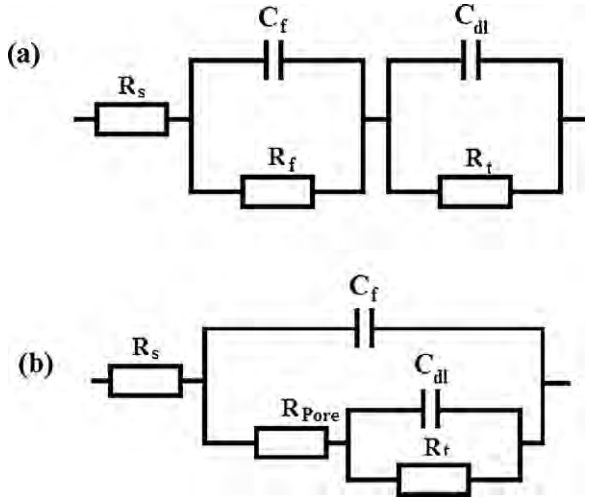

Fig. 8. Equivalent circuits based on analysis of the EIS spectra acquired from the WE43 magnesium alloy soaked in SBF for 5 min: (a) un-implanted WE43 alloy and (b) Al–O implanted WE43 alloy.

Table 1
Fitted EIS results of WE43 magnesium alloy in SBF.

	R_s ($\Omega\,cm^2$)	Y_{0f} ($S\,cm^{-2}\,s^{-n}$)	n_f	R_f or R_{Pore} ($\Omega\,cm^2$)	Y_{0d1} ($S\,cm^{-2}\,s^{-n}$)	n_{dl}	R_t ($\Omega\,cm^2$)
Un-implanted	36.96	6.333E−5	0.7597	32.98 (R_f)	6.765E−3	0.9267	8.792
Al–O implanted	26.71	1.063E−6	0.9254	1217 (R_{Pore})	5.196E−4	0.9933	93.45

The high degradation rates of commercial magnesium alloys in SBF primarily originate from aggressive attack by chloride ions. It is known that MgO can react slowly with H_2O to produce $Mg(OH)_2$. Because $Mg(OH)_2$ is slightly soluble in an aqueous solution and chloride ions can transform it into more soluble $MgCl_2$ [38], the protective effect of the oxide film is compromised and further dissolution of magnesium is promoted. Similarly, sulfates, phosphates, and carbonates in the SBF can also attack magnesium, but not to the extent of chloride ions. Unlike $Mg(OH)_2$ and MgO, Al_2O_3 is relatively stable in the aqueous medium and can effectively resist attack by chloride ions. Hence, formation of the Al_2O_3-containing surface layer provides a good barrier to improve the corrosion resistance of the WE43 alloy in chloride-containing solutions. Although the modified layer is not very thick, significant improvement in the corrosion resistance has already been achieved. Further optimization of the processing parameters is expected to produce better results and based on this study, Al and O dual ion implantation is a promising surface modification technique for WE43 magnesium alloy.

4. Conclusion

An Al oxide-containing surface structure is produced on Mg-Y-RE magnesium alloy using Al–O dual ion implantation. After the surface treatment, the corrosion resistance in simulated body fluids is significantly improved as indicated by polarization test and electrochemical impedance spectroscopy. Our study reveals that localized corrosion becomes the dominant corrosion mechanism instead of general corrosion after surface modification.

Acknowledgements

This work was jointly supported by HKU Seed Funding for Basic Research as well as RGC GRFs #718507, #123708 and #112501.

References

[1] Q. Peng, Y. Huang, L. Zhou, N. Hort, K.U. Kainer, Biomaterials 31 (2010) 398.
[2] F. Witte, V. Kaese, H. Haferkamp, E. Switzer, Biomaterials 26 (2005) 3557.
[3] E. Zhang, D. Yin, L. Xu, L. Yang, K. Yang, Mater. Sci. Eng. C 29 (2009) 987.
[4] X. Gu, Y. Zheng, S. Zhong, T. Xi, J. Wang, W. Wang, Biomaterials 31 (2010) 1093.
[5] M.P. Staiger, A.M. Pietak, J. Huadmai, G. Dias, Biomaterials 27 (2006) 1728.
[6] P. Erne, M. Schier, T.J. Resink, Cardiovasc. Intervent. Radiol. 29 (2006) 11.
[7] A.C. Hänzi, P. Gunde, M. Schinhammer, P.J. Uggowitzer, Acta Biomater. 5 (2009) 162.
[8] O.I. Velikokhatnyi, P.N. Kumta, Acta Biomater. 6 (2010) 1698.
[9] A. Drynda, N. Deinet, N. Braun, M. Peuster, J. Biomed. Mater. Res. A 91A (2009) 360.
[10] F. Feyerabend, J. Fischer, J. Holtz, F. Witte, R. Willumeit, H. Drücker, C. Vogt, N. Hort, Acta Biomater. 6 (2010) 1834.
[11] C. Mario, H. Griffiths, O. Goktekin, N. Peeters, J. Verbist, M. Bosiers, et al., J. Interven. Cardiovasc. 17 (2004) 391.
[12] J. Ormiston, M. Webster, Lancet 369 (2007) 1839.
[13] V. Birss, S. Xia, R. Yue, R.G. Rateick Jr., J. Electrochem. Soc. 151 (2004) B1.
[14] M.C. Turhan, R.P. Lynch, H. Jha, P. Schmuki, S. Virtanen, Electrochem. Commun. 12 (2010) 796.
[15] H.M. Wong, K.W.K. Yeung, K.O. Lam, V. Tama, P.K. Chu, K.D.K. Luk, K.M.C. Cheung, Biomaterials 31 (2010) 2084.
[16] N. Iranipour, R.A. Khosroshahi, N.P. Ahmadi, Surf. Coat. Technol. 205 (2010) 2281.
[17] G. Wu, X. Zeng, G. Li, S. Yao, X. Wang, Mater. Lett. 60 (2006) 674.
[18] R. Xu, G. Wu, X. Yang, T. Hu, Q. Lu, P.K. Chu, Mater. Lett. 65 (2011) 2171.
[19] G. Wu, L. Gong, K. Feng, S. Wu, Y. Zhao, P.K. Chu, Mater. Lett. 65 (2011) 661.
[20] X. Wang, X. Zeng, G. Wu, S. Yao, Y. Lai, J. Alloys Compd. 437 (2007) 87.
[21] X.M. Wang, X.Q. Zeng, G.S. Wu, S.S. Yao, Y.J. Lai, J. Alloys Compd. 456 (2008) 384.
[22] J.E. Gray, B. Luan, J. Alloys Compd. 336 (2002) 88.
[23] P.K. Chu, Surf. Coat. Technol. 201 (2007) 5601.
[24] P.K. Chu, J. Vac. Sci. Technol. B 22 (2004) 289.
[25] C. Liu, Y. Xin, X. Tian, J. Zhao, P.K. Chu, J. Vac. Sci. Technol. A 25 (2007) 334.
[26] Y.C. Xin, C.L. Liu, W.J. Zhang, J. Jiang, G.Y. Tang, X.B. Tian, K.P. Chu, J. Electrochem. Soc. 155 (2008) C178.
[27] H. Fischert, C. Niedhart, N. Kaltenborn, A. Prange, R. Marx, F.U. Niethard, R. Telle, Biomaterials 26 (2005) 6151.
[28] Y. Tao, T. Xiong, C. Sun, H. Jin, H. Du, T. Li, Appl. Surf. Sci. 256 (2009) 261.
[29] S.W. Lee, C. Morillo, J.L. Olivares, S.H. Kim, T. Sekino, K. Niihara, B.J. Hockey, Wear 255 (2003) 1040.
[30] G. Willmann, H.J. Früh, H.G. Pfaff, Biomaterials 17 (1996) 2157.
[31] P. Thomas, S. Barnstorf, B. Summer, G. Willmann, B. Przybilla, Biomaterials 24 (2003) 959.
[32] B. Fartash, T. Tangerud, J. Silness, K. Arvidson, Clin. Oral Implants Res. 7 (1996) 220.
[33] J. Zhang, W. Zhang, C. Yan, K. Du, F. Wang, Electrochim. Acta 55 (2009) 560.
[34] T. Kokubo, H. Kushitani, S. Sakka, T. Kitsugi, T. Yamamuro, J. Biomed. Mater. Res. 24 (1990) 721.
[35] M. Liu, S. Zanna, H. Ardelean, I. Frateur, P. Schmutz, G. Song, A. Atrens, P. Marcus, Corros. Sci. 51 (2009) 1115.
[36] Y. Song, D. Shan, R. Chen, F. Zhang, E. Han, Mater. Sci. Eng. C 29 (2009) 1039.
[37] Y.J. Zhang, C.W. Yan, F.H. Wang, W.F. Li, Corros. Sci. 47 (2005) 2816.
[38] Y.C. Xin, K.F. Huo, T. Hu, G.Y. Tang, P.K. Chu, Acta Biomater. 4 (2008) 2008.